Fano resonance and flux-dependent transport through a triple-arm Aharonov–Bohm interferometer under an applied electric field

2007 J. Phys.: Condens. Matter 19 496219

(http://iopscience.iop.org/0953-8984/19/49/496219)

IOP PUBLISHING JOURNAL OF PHYSICS: CONDENSED MATTER

J. Phys.: Condens. Matter **19** (2007) 496219 (9pp) doi:10.1088/0953-8984/19/49/496219

Fano resonance and flux-dependent transport through a triple-arm Aharonov–Bohm interferometer under an applied electric field

Y X Li

College of Physics, Hebei Normal University, Shijiazhuang 050016, People's Republic of China
and
Asia Pacific Center for Theoretical Physics (APCTP), POSTECH, Pohang 790-784, Korea

Received 27 July 2007, in final form 24 October 2007
Published 15 November 2007
Online at stacks.iop.org/JPhysCM/19/496219

Abstract

The electron transport through a triple-arm Aharonov–Bohm (TAAB) interferometer with an electron–electron interaction quantum dot embedded in each arm is studied using the Green's function technique by means of self-consistent calculation. Transport through one arm of the TAAB interferometer provides the 'background channel'. Linear conductance shows a symmetric structure including the effect of the Coulomb blockade, even in the out-of-equilibrium state, by applying a finite voltage across the device. Four Fano resonant peaks appear with an opposite Fano factor in the conductance, which is different from that of the double-quantum-dot AB interferometer. Not only the magnitude but also the sign of the Fano factor can be controlled more easily when the energy levels of the quantum dots in the reference arm are modified by adjusting the gate or the bias voltage in experiments. As a function of the magnetic field, the AB oscillation is also affected considerably.

1. Introduction

Transport through quantum dots (QDs) has been studied extensively and has revealed interesting phenomena such as resonant tunneling, Coulomb blockade, and the Kondo effect [1–3]. On the other hand, quantum coherence is detected through an Aharonov–Bohm (AB) interferometer. Tunneling through an AB interferometer, an electron moving from the left-hand reservoir to the right-hand reservoir, is split into two partial waves which interfere with each other. In order to measure the interplay of the resonant transport, in particular the electron–electron interaction and quantum coherence, an AB ring with one quantum dot embedded in its arm has been the subject of active research during the past ten years [4–6].

When the discrete energy level in the quantum dot is embedded in a continuum energy state of the electrode, an asymmetric line shape in the linear conductance arises around the discrete quantum dot level as a function of the gate or bias voltage, which is called the well-known Fano effect [7]. Scanning tunneling microscopy measurements of magnetic atoms

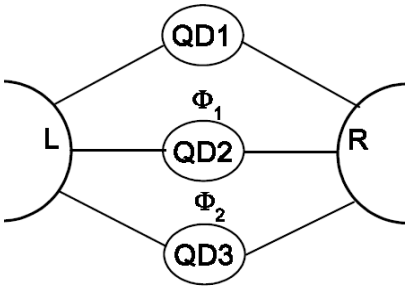

Figure 1. The model of the triple-arm Aharonov–Bohm interferometer. A quantum dot with electron–electron interaction embedded in each arm.

on gold surfaces yielded Fano line shapes in the tunneling density of states, which have been successfully explained theoretically under the assumption that only conduction electrons participate in tunneling [8–10].

Beside containing one quantum dot, an AB interferometer containing a double quantum dot (DQD) has been investigated, and some new interference effects have been found [11–17]. de Guevara *et al* [11] have investigated transport through a DQD with interdot coupling and found that a progressive reduction of tunneling through the antibonding state takes place when the DQD system undergoes a transition from serial to parallel alignment. Lu *et al* [15] also studied the DQD system and found that, by adjusting the magnetic flux, the function of two quantum states can be exchanged, giving rise to the so-called swap effect.

We have investigated a serial-coupled double-ring AB interferometer [18] and found that the zero-bias conductance varies non-monotonically due to coupling between the two rings, which is different from the case of a single-ring AB interferometer. Very recently, de Guevara and Orellana [19] proposed a parallel-coupled triple quantum dot molecule; Fano resonances and bound states in continuum (BIC) were investigated. In experiment, the Kondo line shape can be measured as a function of the interatomic distance between Co adatoms in trimer configurations on a Cu single-crystal surface using scanning tunneling spectroscopy (STS) spectra [20]. Motivated by these theoretical predictions and experimental phenomena, in this paper we investigate a three-arm Aharonov–Bohm (TAAB) interferometer with a Coulomb-blockaded quantum dot embedded in each arm (see figure 1), and electron–electron interaction is considered. Using the Green's function method, the linear conductance is calculated numerically. With transport through one or two arms as a background channel, the linear conductance shows a typical Fano resonance, and the Fano factor changes when the energy levels of the reference quantum dots are modulated by the gate or bias voltage. By applying a finite bias across the device, the state of the quantum dots can be driven out of equilibrium, but by adjusting the quantum dot energies in this TAAB device using an appropriate method, the shape of the conductance stays in symmetry.

This paper is organized as follows. In section 2 we discuss the Hamiltonian of a general TAAB device and derive the formula for linear conductance. We then analyze, in section 3, the quantum-transport properties of the structure in our model. Finally, section 4 summarizes the results of our work.

2. Model and formulas

The TAAB interferometer that we examine in the present work is shown in figure 1. It consists of an AB ring with three arms, and a quantum dot with electron–electron interaction embedded

in each arm; the AB ring is connected by two electrodes to the outside world. The Hamiltonian of the system can be written as

$$H = H_{\mathrm{L}} + H_{\mathrm{R}} + H_{\mathrm{D}} + H_{\mathrm{T}}, \tag{1}$$

where H_{L} and H_{R} are the Hamiltonians for the left-hand ($v = L$) and the right-hand ($v = R$) leads:

$$H_v = \sum_{k,\sigma} \epsilon_{kv\sigma} a^+_{kv\sigma} a_{kv\sigma}. \tag{2}$$

Here $a_{kv\sigma}$ ($a^+_{kv\sigma}$) denotes the annihilation (creation) operator for electrons in the lead v with energy $\epsilon_{kv\sigma}$. H_{D} describes the dynamics of the three quantum dots:

$$H_{\mathrm{D}} = \sum_{\sigma,i=1-3} \epsilon_i d^+_{i\sigma} d_{i\sigma} + \sum_{i=1-3} U_i n_{i\uparrow} n_{i\downarrow}, \tag{3}$$

where $d^+_{i\sigma}$ ($d_{i\sigma}$) represents the creation (annihilation) operator of the electron with energy ϵ_i, U_i is the intradot electron–electron interaction, and $n_{i\sigma} = d^+_{i\sigma} d_{i\sigma}$ is the occupation per spin σ for the dot i. Finally, H_{T} is the tunneling between the dots and the two electrodes:

$$H_{\mathrm{T}} = \sum_{k,v,i,\sigma} (T_{k,v,i} a^+_{kv\sigma} d_{i\sigma} + \mathrm{H.c.}), \tag{4}$$

where T_{kvi} are the tunneling matrix elements. The retarded Green's function $\mathbf{G}^{\mathrm{R}}(\epsilon)$ is a 3×3 matrix,

$$\mathbf{G}^{\mathrm{R}}(\epsilon) = \begin{pmatrix} G^{\mathrm{R}}_{11}(\epsilon) & G^{\mathrm{R}}_{12}(\epsilon) & G^{\mathrm{R}}_{13}(\epsilon) \\ G^{\mathrm{R}}_{21}(\epsilon) & G^{\mathrm{R}}_{22}(\epsilon) & G^{\mathrm{R}}_{23}(\epsilon) \\ G^{\mathrm{R}}_{31}(\epsilon) & G^{\mathrm{R}}_{32}(\epsilon) & G^{\mathrm{R}}_{33}(\epsilon) \end{pmatrix}, \tag{5}$$

with the definition

$$G^{\mathrm{R}}_{ij} \equiv \langle\langle d_{i\sigma} | d^+_{j\sigma} \rangle\rangle_\epsilon \equiv -\mathrm{i} \int \mathrm{e}^{\mathrm{i}\omega t} \langle \{ d_{i\sigma}(t), d^+_{j\sigma}(0) \} \rangle \, \mathrm{d}t. \tag{6}$$

Here, $\{,\}$ and $\langle\rangle$ denote the anti-commutator and statistical average of operators, respectively. $\langle\langle d_{i\sigma} | d^+_{j\sigma} \rangle\rangle_\epsilon$ can be resolved by equation of motion:

$$(\epsilon - \epsilon_i) \langle\langle d_{i\sigma} | d^+_{j\sigma} \rangle\rangle_\epsilon = \delta_{ij} + \sum_{kv} T_{kvi} \langle\langle a_{kv\sigma} | d^+_{j\sigma} \rangle\rangle_\epsilon + U_i \langle\langle d_{i\sigma} n_{-\sigma} | d^+_{j\sigma} \rangle\rangle_\epsilon. \tag{7}$$

Applying the equation of motion to the Green's functions on the right-hand side of equation (7), we can find

$$(\epsilon - \varepsilon_{kv\sigma}) \langle\langle a_{kv\sigma} | d^+_{j\sigma} \rangle\rangle_\epsilon = \sum_{ki} T_{kvi} \langle\langle d_{i\sigma} | d^+_{j\sigma} \rangle\rangle_\epsilon, \tag{8}$$

$$\begin{aligned}(\epsilon - \epsilon_i - U_i) \langle\langle d_{i\sigma} n_{i-\sigma} | d^+_{j\sigma} \rangle\rangle_\epsilon &= \langle n_{i-\sigma} \rangle \delta_{ij} + \sum_{kv} [T_{kvi} \langle\langle a_{kv\sigma} n_{i-\sigma} | d^+_{j\sigma} \rangle\rangle_\epsilon \\ &\quad - T_{kv-\sigma} \langle\langle d_{i\sigma} a^+_{kv-\sigma} d_{i-\sigma} | d^+_{j\sigma} \rangle\rangle_\epsilon + T_{kv-\sigma} \langle\langle d_{i\sigma} d^+_{i-\sigma} a_{kv-\sigma} | d^+_{j\sigma} \rangle\rangle_\epsilon].\end{aligned} \tag{9}$$

Now, the Hartree–Fock decoupling scheme is applied to the higher-order Green's functions generated on the right-hand side of equation (9),

$$\langle\langle a_{kv\pm\sigma} n_{i-\sigma} | d^+_{j\sigma} \rangle\rangle_\epsilon \to \langle n_{i-\sigma} \rangle \langle\langle a_{kv\pm\sigma} | d^+_{j\sigma} \rangle\rangle_\epsilon, \tag{10}$$

$$\langle\langle d_{i\sigma} a_{kv\pm\sigma} d^+_{i-\sigma} | d^+_{j\sigma} \rangle\rangle \to \langle d^+_{i-\sigma} d_{i\sigma} \rangle \langle\langle a_{kv\pm\sigma} | d^+_{j\sigma} \rangle\rangle, \tag{11}$$

$$\langle\langle d_{i\sigma} a^+_{kv\pm\sigma} d_{i-\sigma} | d^+_{j\sigma} \rangle\rangle \simeq 0, \tag{12}$$

which closes the set of equations (7)–(9) and allows us to find a solution for the Green's functions $G^{\mathrm{R}}_{ij}(\epsilon)$.

The general solution for the Green's function may be written in the compact form of the matrix Dyson equation,

$$\mathbf{G}^{\mathrm{R}}(\epsilon) = [\mathbf{1} - \mathbf{g}^{\mathrm{R}}(\epsilon)\mathbf{\Sigma}^{\mathrm{R}}(\epsilon)]^{-1}\mathbf{g}^{\mathrm{R}}(\epsilon), \tag{13}$$

where $\mathbf{g}^{\mathrm{R}}(\epsilon)$ is the corresponding Green's function of the dot decoupled from the electrodes, but with the Coulomb interaction,

$$g_{ij}^{R}(\epsilon) = \frac{\epsilon - \varepsilon_i - U_i(1 - \langle n_{i-\sigma}\rangle)}{(\epsilon - \varepsilon_i)(\epsilon - \varepsilon_i - U_i)}\delta_{ij}. \tag{14}$$

The self-energy $\mathbf{\Sigma}^{\mathrm{R}}(\epsilon)$ includes two terms,

$$\mathbf{\Sigma}^{\mathrm{R}}(\epsilon) = \mathbf{\Sigma}_l^{\mathrm{R}}(\epsilon) + \mathbf{\Sigma}_r^{\mathrm{R}}(\epsilon), \tag{15}$$

and $\Sigma_v^{\mathrm{R}}(\epsilon) = -\mathrm{i}\Gamma_v/2$, where Γ_v is the tunneling coupling matrix.

We neglect the energy dependence of the tunnel matrix elements and assume a symmetric coupling strength: $T_{kL1} = |t|\mathrm{e}^{\mathrm{i}\phi_1/4}$, $T_{kL2} = |t|\mathrm{e}^{\mathrm{i}\phi_2/4}$, $T_{kL3\sigma} = |t|\mathrm{e}^{\mathrm{i}\phi_3/4}$, $T_{kR1} = |t|\mathrm{e}^{-\mathrm{i}\phi_1/4}$, $T_{kR2} = |t|\mathrm{e}^{-\mathrm{i}\phi_2/4}$, $T_{kR3} = |t|\mathrm{e}^{-\mathrm{i}\phi_3/4}$. For the phase shift due to the total magnetic flux threading into the TAAB interferometer, we choose a symmetric gage such that $\phi_1 = 2\pi(\Phi_1 + \Phi_2)/\Phi_0$, $\phi_2 = 2\pi(\Phi_1 - \Phi_2)/\Phi_0$, and $\phi_3 = -2\pi(\Phi_1 + \Phi_2)/\Phi_0$, where Φ_1, Φ_2 are the applied magnetic field (see figure 1) and the flux quantum $\Phi_0 = hc/e$. In our calculation, we define the linewidth matrix as $\Gamma_{ij}^{v} = \sum_k T_{kvi}T_{kvj}^{*}2\pi\delta(\varepsilon - \varepsilon_{kv\sigma})$. Thus, in the 3×3 generalized Nambu space, the tunneling coupling matrix is described by

$$\Gamma_{\mathrm{L}} = \begin{pmatrix} \Gamma_1^{\mathrm{L}} & \sqrt{\Gamma_1^{\mathrm{L}}\Gamma_2^{\mathrm{L}}}\mathrm{e}^{\mathrm{i}(\phi_1-\phi_2)} & \sqrt{\Gamma_1^{\mathrm{L}}\Gamma_3^{\mathrm{L}}}\mathrm{e}^{\mathrm{i}(\phi_1-\phi_3)} \\ \sqrt{\Gamma_1^{\mathrm{L}}\Gamma_2^{\mathrm{L}}}\mathrm{e}^{-\mathrm{i}(\phi_1-\phi_2)} & \Gamma_2^{\mathrm{L}} & \sqrt{\Gamma_2^{\mathrm{L}}\Gamma_3^{\mathrm{L}}}\mathrm{e}^{\mathrm{i}(\phi_2-\phi_3)} \\ \sqrt{\Gamma_1^{\mathrm{L}}\Gamma_3^{\mathrm{L}}}\mathrm{e}^{-\mathrm{i}(\phi_1-\phi_3)} & \sqrt{\Gamma_2^{\mathrm{L}}\Gamma_3^{\mathrm{L}}}\mathrm{e}^{-\mathrm{i}(\phi_2-\phi_3)} & \Gamma_3^{\mathrm{L}} \end{pmatrix}, \tag{16}$$

and

$$\Gamma_{\mathrm{R}} = \begin{pmatrix} \Gamma_1^{\mathrm{R}} & \sqrt{\Gamma_1^{\mathrm{R}}\Gamma_2^{\mathrm{R}}}\mathrm{e}^{-\mathrm{i}(\phi_1-\phi_2)} & \sqrt{\Gamma_1^{\mathrm{R}}\Gamma_3^{\mathrm{R}}}\mathrm{e}^{-\mathrm{i}(\phi_1-\phi_3)} \\ \sqrt{\Gamma_1^{\mathrm{R}}\Gamma_2^{\mathrm{R}}}\mathrm{e}^{\mathrm{i}(\phi_1-\phi_2)} & \Gamma_2^{\mathrm{R}} & \sqrt{\Gamma_2^{\mathrm{R}}\Gamma_3^{\mathrm{R}}}\mathrm{e}^{-\mathrm{i}(\phi_2-\phi_3)} \\ \sqrt{\Gamma_1^{\mathrm{R}}\Gamma_3^{\mathrm{R}}}\mathrm{e}^{\mathrm{i}(\phi_1-\phi_3)} & \sqrt{\Gamma_2^{\mathrm{R}}\Gamma_3^{\mathrm{R}}}\mathrm{e}^{\mathrm{i}(\phi_2-\phi_3)} & \Gamma_3^{\mathrm{R}} \end{pmatrix}. \tag{17}$$

Here, Γ_i^v is short for Γ_{ii}^v.

The correlation Green's function $\mathbf{G}^{<}(\epsilon)$ can be calculated from the Keldysh equation [21],

$$\mathbf{G}^{<}(\epsilon) = \mathbf{G}^{R}(\epsilon)\mathbf{\Sigma}^{<}(\epsilon)\mathbf{G}^{A}(\epsilon), \tag{18}$$

where the lesser self-energy $\mathbf{\Sigma}^{<}(\epsilon)$ is related to the retarded and the advanced self-energies,

$$\mathbf{\Sigma}^{<}(\epsilon) = -\sum_{v}[\mathbf{\Sigma}_v^{\mathrm{R}}(\epsilon) - \mathbf{\Sigma}_v^{A}(\epsilon)]f_v(\epsilon), \tag{19}$$

where $f_v(\epsilon)$ is the Fermi–Dirac distribution function for the vth electrode, $f_v(\epsilon) = 1/\{1 + \exp[(\epsilon - \mu_v)/k_{\mathrm{B}}T]\}$, with the electrochemical potentials $\mu_l = eV_l = eV/2$ and $\mu_r = eV_r = -eV/2$, respectively.

The average values of the occupation numbers $\langle n_{i\sigma}\rangle = \langle d_{i\sigma}^{+}d_{i\sigma}\rangle$, which enter the expressions for the Green's functions, has to be calculated self-consistently using the formulas

$$\langle n_{i\sigma}\rangle = \mathrm{Im}\int_{-\infty}^{+\infty}\frac{\mathrm{d}\epsilon}{2\pi}G_{ii}^{<}(\epsilon). \tag{20}$$

The differential conductance $G = \mathrm{d}I/\mathrm{d}V$ is related to the effective transmission, and now can be calculated as [21, 22]

$$G = \frac{2e^2}{h}\int \mathrm{d}\epsilon\left(-\frac{\partial f}{\partial \epsilon}\right)\mathrm{Tr}\left\{\frac{\Gamma_{\mathrm{R}}(\epsilon)\Gamma_{\mathrm{L}}(\epsilon)}{\Gamma_{\mathrm{R}}(\epsilon) + \Gamma_{\mathrm{L}}(\epsilon)}[G^{\mathrm{R}}(\epsilon) - G^{A}(\epsilon)]\right\}. \tag{21}$$

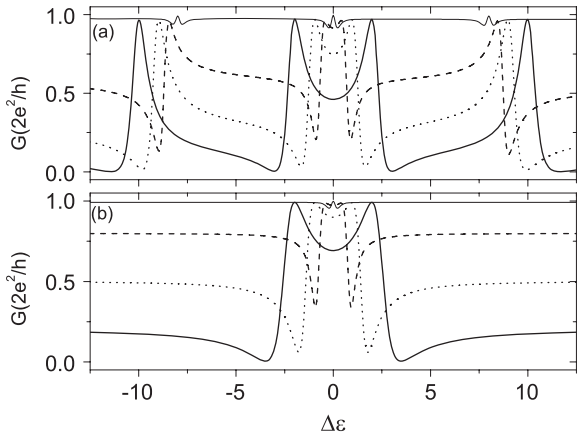

Figure 2. The linear conductance as a function of $\Delta\epsilon$ with and without electron–electron interaction: (a) $U = 8$ and (b) $U = 0$. The thin solid, dashed, dotted, and thick solid lines correspond to $\epsilon_2 = 0.0$, 0.5, 1.0, and 2.0, respectively.

3. Results and discussion

In the present paper, a symmetric structure $\Gamma_i^L = \Gamma_i^R = \Gamma$ is considered; Γ is taken as the energy unit. The magnetic field is assumed to be $\Phi_1 = \Phi_2$, i.e., $\phi_1 = -\phi_3$ and $\phi_2 = 0$. In the following calculation, we define the magnetic field $\phi_1 = -\phi_3 = \phi/4$ and electron–electron interaction $U = 8\Gamma$, respectively.

First of all, we fix the energy level of quantum dot 2 (QD2), i.e. ϵ_2, and vary the other energy levels $\epsilon_1 (= \epsilon_2 - \Delta\epsilon)$ and $\epsilon_3 (= \epsilon_2 + \Delta\epsilon)$; the magnetic field and the bias are not considered. The linear conductance as a function of $\Delta\epsilon$ is calculated and the result is shown in figure 2(a). For comparison, the case of non-electron–electron interaction is also indicated in figure 2(b). From figure 2 we find that, with and without electron–electron interaction, when the quantum dot energy level $\epsilon_2 = 0.0$, the electrons can tunnel through the device much more easily, and the conductance maintains a high value. When there is no electron–electron interaction, i.e. $U = 0$, we can see in figure 2(b) that the conductance shows a typical Fano resonant shape due to interference of the electrons passing through the different arms of the AB interferometer, which is in agreement with previous theoretical and experimental studies. Transport through QD2 provides the 'background channel' with transmission $T_b = \Gamma^2/[\epsilon_2^2 + \Gamma^2]$; two symmetric Fano resonances appear at $\Delta\epsilon = \pm\epsilon_2$ with an opposite Fano factor.

When the electron–electron interaction is considered, the quantum dot energy level will be renormalized. We can see from figure 2(a) that four Fano resonances arise at $\Delta\epsilon = \pm\epsilon_2$, $\pm(\epsilon_2 + U)$. Due to the Coulomb blockade, the electrons can flow only when electrons in the electrodes have sufficient energy to occupy the lowest possible energy states. By changing the energies of the quantum dots, the energy level of the dot states is shifted through the Fermi energy of the electrodes. This leads to a series of peaks in the conductance. Between the two peaks at $\Delta\epsilon = \epsilon_2$ and $\epsilon_2 + U$ (and also at $\Delta\epsilon = -\epsilon_2$ and $-\epsilon_2 - U$), the conductance is suppressed because the electrons in the electrodes have insufficient energy to overcome the Coulomb repulsion; the Coulomb blockade effect appears. We can also see that, when ϵ_2 is zero, the peak of the conductance is symmetrical; the Fano factor is zero. When the energy level ϵ_2 increases, the asymmetric parameter of the conductance peaks becomes stronger, and

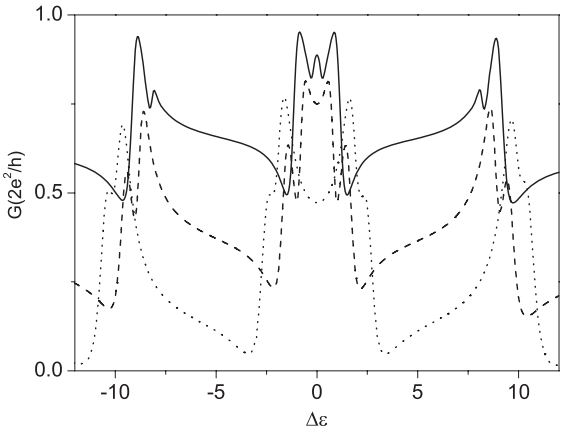

Figure 3. The linear conductance as a function of $\Delta\epsilon$ with electron–electron interaction $U = 8$, $\phi = 0$, and bias $eV = 0.8$. The solid, dashed, and dotted lines correspond to $\epsilon_2 = 0.5$, 1.0, and 2.0, respectively.

the Fano factor increases. It is interesting to note that in this three-arm model, if we fix one quantum dot energy, there are another two quantum dots in which energies can be modulated; as a result, the Fano factor varies symmetrically. It can be seen in figure 2(a) that at $\Delta\epsilon = \epsilon_2$, $\epsilon_2 + U$ the Fano factor is positive, but at $\Delta\epsilon = -\epsilon_2$, $-(\epsilon_2 + U)$, the Fano factor becomes negative, but with the same absolute value.

When a finite bias is applied across the TAAB interferometer, the conductance is as indicated in figure 3. The electric field drives the system out of equilibrium, enriching the interplay between quantum coherence and the electron–electron interaction. In addition to the main peaks related to the quantum dot energies, new satellite resonant peaks appear at the energy side. Because the electric field applied across the device is small, $eV = 0.1U$, when the energy of quantum dot 2 (ϵ_2) becomes large (see the dotted line in figure 3), the effect of the bias voltage on the transport becomes weak. It is natural to expect that the transport symmetry present at the equilibrium state may be broken due to the applied electric field. But, for the present model, we vary the energy levels of quantum dot 1 and quantum dot 3 synchronously; the symmetry of the conductance is not broken even in this non-equilibrium system.

For the same time, we calculate the conductance as a function of the energy level of quantum dot 2, ϵ_2, and fix energy levels ϵ_1 and ϵ_3; the result is plotted in figure 4. Transport through quantum dot 1 and quantum dot 3 acts as the 'background channel':

$$T_{\mathrm{b}} = \frac{\Gamma[(\epsilon_1+\epsilon_3)^2\cos^2\frac{\phi}{2} + \Delta\epsilon^2\sin^2\frac{\phi}{2}]}{[(\frac{\epsilon_1+\epsilon_3}{2})^2 - (\frac{\delta\epsilon}{2})^2 - \Gamma^2\sin^2\frac{\phi}{2}]^2 + (\epsilon_1+\epsilon_3)^2\Gamma}. \tag{22}$$

In this case, the energy level $\epsilon_1 = -\epsilon_3$ is defined; thus, in figure 4(a) we can find that the positions of the Fano resonant peaks are fixed at $\epsilon_2 = 0,\ U$, and do not shift when the energy levels of quantum dot 1 and quantum dot 3 are modified. This condition will be changed when a finite bias is applied across the device; one can see in figure 4(b) that the peaks of the conductance shift accordingly. We can simulate the shape of the conductance using the generalized Fano form, $T \sim \frac{(\epsilon+q)^2}{\epsilon^2+1}$, at the Fermi level, where q is the Fano factor. When the energy difference between quantum dot 1 and quantum dot 3 becomes larger, the Fano resonance of the conductance is sharper, and the Fano factor becomes bigger. Thus, the Fano factor can be strongly affected by adjusting the energies of the reference dots using the gate voltage.

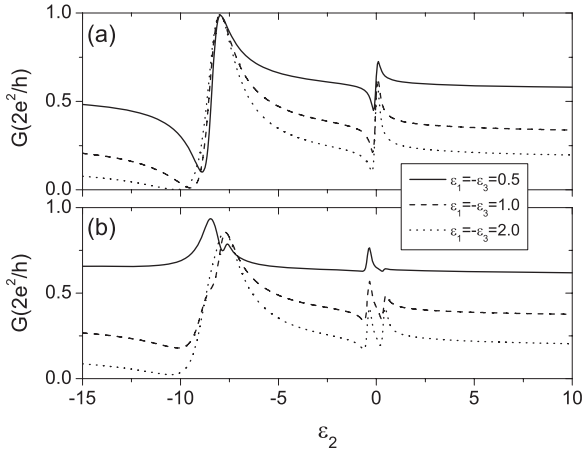

Figure 4. The linear conductance as a function of ϵ_2 with different values of the energy levels of QD1 and QD3, $U = 8$ and $\phi = 0$, respectively: (a) $eV = 0.0$ and (b) $eV = 0.8$.

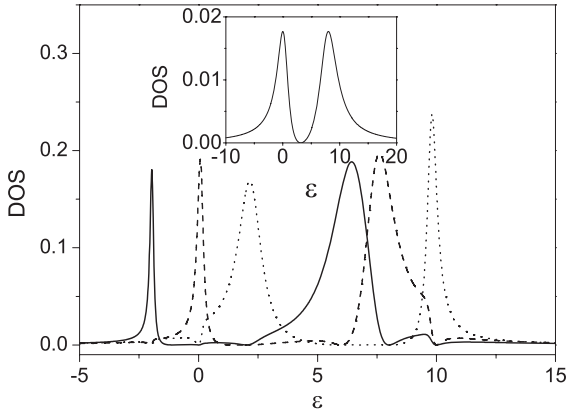

Figure 5. Density of states as a function of the energy for three quantum dots, $U = 8$, $\phi = 0$, and $eV = 0$. Solid, dashed, and dotted lines correspond to QD1, QD2, and QD3, respectively. Inset: $\epsilon_1 = \epsilon_2 = \epsilon_3 = 0.0$.

Now we examine the density of states (DOS) of the quantum dots. Figure 5 shows the calculated density of state of the three quantum dots for the condition $\epsilon_1 = -\epsilon_3 = 2.0$, $\epsilon_2 = 0.0$, $\varphi = 0$. The inset is the case $\epsilon_1 = \epsilon_3 = \epsilon_2 = 0.0$. When the three dots have the same energy levels, ϵ_0 for example, the local density of states in each quantum dot is the same, and the electron has the same probability of being found. The DOS inset of figure 5 shows two binding states. The first one is located at the energy $\epsilon = \epsilon_0$, the energy required to put the first electron in the QD. The second resonance appears at $\epsilon = \epsilon_0 + U$, the energy required to add an additional electron. The shape of the resonance peaks is Lorentzian, which contributes two Breit–Wigner peaks to the conductance. When the energy levels for the dots are different, quantum interference effects arise. The Lorenztian at the bonding energy produces a Breit–Wigner shape to the conductance, while that at the anti-bonding energy becomes a δ function, giving a Fano effect. Because the three quantum dots connect with the same source and drain electrodes and have interactions with each other, we can find in figure 5 that the DOS

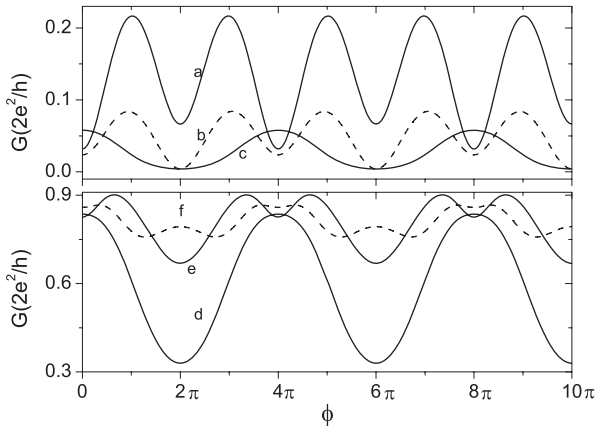

Figure 6. AB oscillations for different values of $(\epsilon_1, \epsilon_2, \epsilon_3)$, with $U = 8$ and $eV = 0.8$: $a(-4.0, -2.0, 0.0)$, $b(-3.5, -2.0, -0.5)$, $c(-3.0, -2.0, -1.0)$, $d(0.5, 0.0, 0.5)$, $e(-0.5, 0.0, 0.5)$, $f(0.0, 2.0, 4.0)$.

has some anti-resonances, which contributes to the Fano effect making the conductance more complicated.

The AB oscillation is indicated in figure 6. The conductance oscillates as a function of magnetic flux with different periods when the energy levels of the quantum dots are changed. We first see the top panel of figure 6, in which $\epsilon_2 = -2.0$ and $\epsilon_1 = -\epsilon_3 = \epsilon_2 \pm \Delta\epsilon$. In these three cases, we can see that the curves a and b oscillate anomalously but with the same frequency and phase. When the energy difference of the dots $\Delta\epsilon$ becomes small (see curve c) the transport is suppressed, the conductance oscillates slowly and the period of the curve becomes twice that of the previous cases. When we increase the energies of the dots, the results are indicated as d, e, and f in figure 6. The conductance clearly increases. Away from the anomaly, the conductance of curve d is sinusoidal, with a period of 4π. Then, changing the energy of quantum dot 1, i.e. curve e, higher harmonic contributions become important, which corresponds to paths through the AB geometry with higher number around the enclosed magnetic flux. The original resonant peaks at $\phi = 0, 4\pi, 8\pi, \ldots$ develop into double peaks. As we continue to increase the energies of the dots, we can see in curve f that the original resonant peaks not only at $\phi = 0, 4\pi, 8\pi, \ldots$ but also at $\phi = 2\pi, 6\pi, 10\pi, \ldots$ split; the conductance oscillates more quickly. Thus, in the present device, by varying the applied magnetic field and the energy of the quantum dot, the frequency, the amplitude, and the phase of the conductance can be controlled.

There are other interactions, such as the electron–phonon interaction etc, which are neglected in the present work. When the electron–phonon interaction is considered, small resonant peaks (sometimes small resonant shoulders) will appear beside the main resonant peaks due to the absorption and emission of phonons. If the temperature is low enough, only the emission processes contributes to the transport behavior; the absorption processes are not available. The strength of the electron–phonon interaction and the frequency of the phonon mode will affect the transport properties simultaneously.

We finally comment on the observability of our proposal and how one can fabricate a TAAB device. A two-arm AB interferometer with a quantum dot embedded in each arm has been set up in experiments [23, 24]. Based on a Ga[Al]As heterostructure with a two-dimensional electron gas (2DEG) below the surface, by using a scanning force microscope the 2DEG is depleted below the oxide lines written on the GaAs surface, thus defining the three-arm

interferometer. A QD is embedded in each arm and the direct tunneling between the dots can be suppressed by applying a negative voltage, which forms the model in the present work.

4. Conclusion

In conclusion, we have investigated the electron transport properties through a TAAB interferometer. The interplay of the electron–electron interaction and quantum coherence plays an important role in the linear conductance. By varying the energy levels of the quantum dots in the different arms, the conductance can be modified, as can the shape of the Fano resonance. The transport properties through triple-arm AB interferometer are quite different to that of the two-arm AB interferometer with one or two quantum dots, especially in the case of an applied bias voltage across the device. By varying the intradot energy level using a gate voltage, the sign of the Fano factor can change from positive to negative, and the amplitude and the frequency of the AB oscillation in the conductance can be controlled more easily. Although we have studied a triple-arm structure, the results that have been obtained can naturally be extended to an AB interferometer with more arms, which gives us more choice to investigate AB devices in experiment.

Acknowledgments

This research was performed during a stay at the Asia Pacific Center for Theoretical Physics (APCTP). This work was also supported by the Natural Science Foundation of China (grant no. 10674040) and the Doctor Subject Foundation of the Ministry of Education, China (grant no. 20060094002).

References

[1] Goldhaber-Gordon D 1998 *Phys. Rev. Lett.* **81** 5225
[2] Cronenwett S M, Oosterkamp T H and Kouwenhoven L P 1998 *Science* **281** 540
[3] Li S S, Xia J B, Yuan Z L, Xu Z Y, Ge W, Wang Y, Wang J and Chang L L 1996 *Phys. Rev.* B **54** 11575
Li S S and Xia J B 1997 *Phys. Rev.* B **55** 15434
Li S S, Chang K, Xia J B and Hirose K 2003 *Phys. Rev.* B **68** 245306
[4] Yacoby A, Heiblum M, Mahalu D and Shtrikman H 1995 *Phys. Rev. Lett.* **74** 4047
[5] Sun Q F, Wang J and Guo H 2005 *Phys. Rev.* B **71** 165310
[6] Baltin R and Gefen Y 1999 *Phys. Rev. Lett.* **83** 5094
[7] Fano U 1961 *Phys. Rev.* **124** 1866
[8] Cooper J R and Wyatt A F G 1973 *J. Phys. F: Met. Phys.* **3** L120
[9] Appelbaum J A 1966 *Phys. Rev. Lett.* **17** 91
[10] Hofstetter W, König J and Schoeller H 2001 *Phys. Rev. Lett.* **87** 156803
[11] de Guevara M L L, Claro F and Orellana P A 2003 *Phys. Rev.* B **67** 195335
[12] Yanaka Y and Kawakami N 2005 *Phys. Rev.* B **72** 085304
[13] Kubala B and König J 2002 *Phys. Rev.* B **65** 245301
[14] Ding G H, Kim C K and Nahm K 2005 *Phys. Rev.* B **71** 205313
[15] Lu H, Lu R and Zhu B F 2005 *Phys. Rev.* B **71** 235320
[16] Peng J, Wang B and Xing D Y 2005 *Phys. Rev.* B **71** 214523
[17] Kang K and Cho S Y 2004 *J. Phys.: Condens. Matter* **16** 117
[18] Li Y X, Choi H Y and Lee H W 2007 *Phys. Lett.* A at press
[19] de Guevara M L and Orellana P A 2006 *Phys. Rev.* B **73** 205303
[20] Wahl P, Simon P, Diekhöner L, Stepanyuk V S, Bruno P, Schneider M A and Kern K 2007 *Phys. Rev. Lett* **98** 056601
[21] Haug H and Jauho A P 1998 *Quantum Kinetics in Transport and Optics of Semiconductors* (Berlin: Springer)
[22] Meir Y and Wingreen N 1992 *Phys. Rev. Lett.* **68** 2512
[23] Sigrist M, Ihn T, Ensslin K, Reinwald M and Wegscheider W 2007 *Phys. Rev. Lett.* **98** 036805
[24] Neder I, Heiblum M, Levinson Y, Mahalu D and Umansky V 2006 *Phys. Rev. Lett.* **96** 016804